

Review

# Recent Progress in Blue Thermally Activated Delayed Fluorescence Emitters and Their Applications in OLEDs: Beyond Pure Organic Molecules with Twist D- $\pi$ -A Structures

Yiting Gao <sup>1,2</sup>, Siping Wu <sup>1</sup>, Guogang Shan <sup>2,\*</sup> and Gang Cheng <sup>1,3,\*</sup>

<sup>1</sup> State Key Laboratory of Synthetic Chemistry, Department of Chemistry, The University of Hong Kong, Hong Kong, China

<sup>2</sup> Institute of Functional Material Chemistry and National & Local United Engineering Lab for Power Battery, Faculty of Chemistry, Northeast Normal University, Changchun 130024, China

<sup>3</sup> HKU Shenzhen Institute of Research and Innovation, Shenzhen 518053, China

\* Correspondence: shangg187@nenu.edu.cn (G.S.); ggcheng@hku.hk (G.C.)

**Abstract:** Thermally activated delayed fluorescence (TADF) materials, which can harvest all excitons and emit light without the use of noble metals, are an appealing class of functional materials emerging as next-generation organic electroluminescent materials. Triplet excitons can be upconverted to the singlet state with the aid of ambient thermal energy under the reverse inter-system crossing owing to the small singlet–triplet splitting energy ( $\Delta E_{ST}$ ). This results from a specific molecular design consisting of minimal overlap between the highest occupied molecular orbital and the lowest unoccupied molecular orbital, due to the spatial separation of the electron-donating and electron-releasing part. When a well-designed device structure is applied, high-performance blue-emitting TADF organic light-emitting diodes can be realized with an appropriate molecular design. Unlike the previous literature that has reviewed general blue-emitting TADF materials, in this paper, we focus on materials other than pure organic molecules with twist D- $\pi$ -A structures, including multi-resonance TADF, through-space charge transfer TADF, and metal-TADF materials. Cutting-edge molecules with extremely small and even negative  $\Delta E_{ST}$  values are also introduced as candidates for next-generation TADF materials. In addition, OLED structures used to exploit the merits of the abovementioned TADF emitters are also described in this review.

**Keywords:** TADF; MR-TADF; TSCT-TADF; metal-TADF; blue OLEDs



**Citation:** Gao, Y.; Wu, S.; Shan, G.; Cheng, G. Recent Progress in Blue Thermally Activated Delayed Fluorescence Emitters and Their Applications in OLEDs: Beyond Pure Organic Molecules with Twist D- $\pi$ -A Structures. *Micromachines* **2022**, *13*, 2150. <https://doi.org/10.3390/mi13122150>

Academic Editor: Jinn-Kong Sheu

Received: 22 October 2022

Accepted: 28 November 2022

Published: 5 December 2022

**Publisher's Note:** MDPI stays neutral with regard to jurisdictional claims in published maps and institutional affiliations.



**Copyright:** © 2022 by the authors. Licensee MDPI, Basel, Switzerland. This article is an open access article distributed under the terms and conditions of the Creative Commons Attribution (CC BY) license (<https://creativecommons.org/licenses/by/4.0/>).

## 1. Introduction

Organic light-emitting diodes (OLEDs) and the use of organic materials in light-emitting technology have caught the attention of researchers since Tang and VanSlyke's pioneering work in 1987 [1] owing to their extraordinary merits, such as high efficiency, light weight, flexibility, and fast response [2–6]. A typical bottom-emitting OLED has a sandwich device structure, in which organic functional layer(s) are sandwiched between a transparent anode and a metal cathode. For high-efficiency OLEDs, the sandwiched functional layers usually consist of a hole-transporting layer (HTL), an emissive layer (EML), and an electron-transporting layer (ETL). In some cases, especially in phosphorescent and thermally activated delayed fluorescent (TADF) OLEDs, one or more auxiliary layers, such as a hole-blocking layer (HBL), a hole-injection layer (HIL), an electron-blocking layer (EBL), and an electron-injection layer (EIL), are added in the stack to further improve device performance. HBLs and HILs are used to confine carriers and excitons in the EML to avoid leaking current and the unwanted recombination of excitons outside the EML, and HIL and EIL are used to facilitate the injection of holes from the anode and electrons from the cathode to lower the driving voltage of the OLED [7]. In some cases, inorganic materials can be employed as HILs and/or EILs, such as MoO<sub>3</sub>, V<sub>2</sub>O<sub>5</sub>, LiF, Cs<sub>2</sub>CO<sub>3</sub>, etc. [8]. Such

a sophisticated device structure is designed to fully exploit the potential of the emitting material, whose photoluminescent quantum yield (PLQY) and decay lifetime determine the performance of a well-designed OLED [9–14].

Light-emitting materials used in OLEDs have advanced rapidly in the last three decades, from fluorescent, phosphorescent, and triplet–triplet annihilation (TTA) materials to TADF materials [15]. Organic electroluminescence (EL) results from the radiative deactivation of excitons from the excited state to the ground state, which can occur with different spin multiplicities such as singlet or triplet excited states, resulting in fluorescence or phosphorescence. When OLEDs work under electrical excitation, singlet and triplet excitons are formed in the EML at a ratio of 1:3 [16], according to spin statistics. The quantum efficiency (QE) of an OLED, which refers to the numerical ratio of photons to injected electron-hole pairs [17], is used to assess its electricity-photon conversion efficiency, which can be further subdivided into internal QE (IQE) and external QE (EQE). IQE, the numerical ratio of total photons generated within the EML to the charge pairs injected, is directly determined by the emitting material [18]. In contrast, EQE is the numerical ratio of total photons emitting out of the device to the charge pairs injected. The chemical structure of the emitter and the associated functional materials can have significant impacts on the device efficiency, since photons are created within and emitted from the EML. IQE of fluorescent OLEDs is limited to 25% in traditional fluorescent emitters, which can only exploit singlet excitons for light emission. On the other hand, phosphorescent emitters that contain noble metals such as platinum, iridium, or osmium can harvest both singlet and triplet excitons through strong spin–orbit coupling, leading to high IQEs of up to 100% in phosphorescent OLEDs [19]. Nonetheless, further application of phosphorescent emitters is limited by the low abundance and high price of noble metals [20]. TTA fluorescent emitters can only achieve a maximum IQE of 62.5% by converting two triplet excitons into one singlet exciton, and their emission is mostly blue [21].

Alternatively, Yersin et al. [22] and Adachi et al. [23] developed inexpensive metal complexes and purely organic molecules, respectively, that are capable of harvesting both singlet and triplet excitons for emission, known as TADF. By reducing the overlap between the molecule's highest occupied molecular orbital (HOMO) and the lowest unoccupied molecular orbital (LUMO), small singlet–triplet splitting ( $\Delta E_{ST}$ ) can be achieved for efficient TADF. After singlet and triplet excitons are formed in the EML, the accumulated triplet excitons in  $T_1$  are transferred to  $S_1$  via a reverse inter-system crossing (RISC) process enhanced by thermal activation in the TADF mechanism [24]. By activating an effective up-conversion process of RISC from an excited triplet state to an excited singlet state, the TADF mechanism can also potentially achieve an IQE of 100% [25–27]. Compounds with suitable donor–acceptor building blocks are usually designed as TADF emitters, in which intramolecular charge transfer (ICT) with a small  $\Delta E_{ST}$  is achieved by donor and acceptor moieties in the same molecule, allowing an effective RISC process to collect singlet emissions by converting triplets to singlets. In addition, twisted molecules, such as phenyl linkers between donors and acceptors, and a clear separation between the HOMO and LUMO distribution benefit TADF [7,9,28,29].

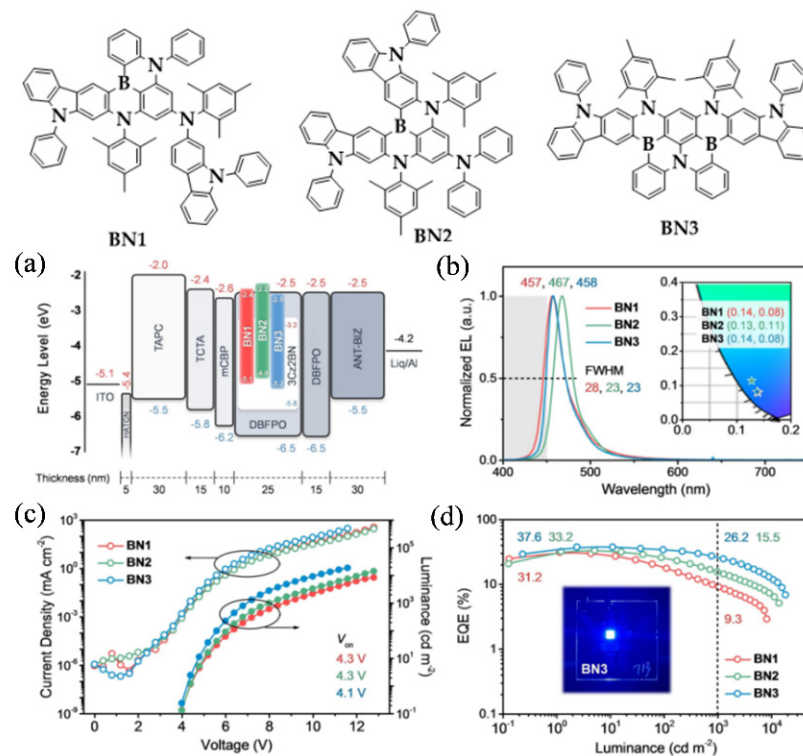
Along with judicious molecular designs, the performance of TADF-OLEDs has made significant progress. Remarkably, researchers have committed their attention to pure blue TADF emitters, which promise to be the final hurdle blocking the achievement of OLEDs for low-cost, highly efficient, and stable display illumination devices [30]. As one of the three primary colors, emitting blue is necessary for both display and lighting applications. However, neither fluorescent nor phosphorescent emitters are suitable candidates for blue OLEDs due to the low efficiency of the former and unsatisfactory stability of the latter. In this regard, TADF emitters could be a possible solution for low-cost, highly efficient, and stable blue OLEDs due to their potential high efficiency and stability. Early reviews have introduced the design concepts, the relationship between molecular structure and photophysical properties, and PL and EL performances of blue TADF materials, most of which are pure organic molecules with twist D- $\pi$ -A structures [9]. However, new

TADF emitters designed with novel concepts reported very recently have been sparsely covered in reviews. In this contribution, we focus on blue TADF materials possessing molecular structures other than pure organic with twist D- $\pi$ -A structures. Recent advances of multiple MR-TADF materials are reviewed in Section 2, especially blue-emitting ones, that potentially address the issues of efficiency roll-off, quenching at high concentrations, and limited operational lifetimes that exist in early MR-TADF emitters. Newly emerged blue TADF emitters from through-space charge transfer (TSCT) processes are introduced in Section 3. A recent development in high-performance blue-emitting metal-TADF materials, especially those based on gold and copper, is briefly presented in Section 4. The outlook and perspective of next-generation TADF emitters with extremely small and even negative  $\Delta E_{ST}$  are predicted in Section 5. In addition, OLED structures that are used to fully exploit the merits of the above-mentioned TADF emitters are also emphasized in this review.

## 2. Blue MR-TADF Emitters

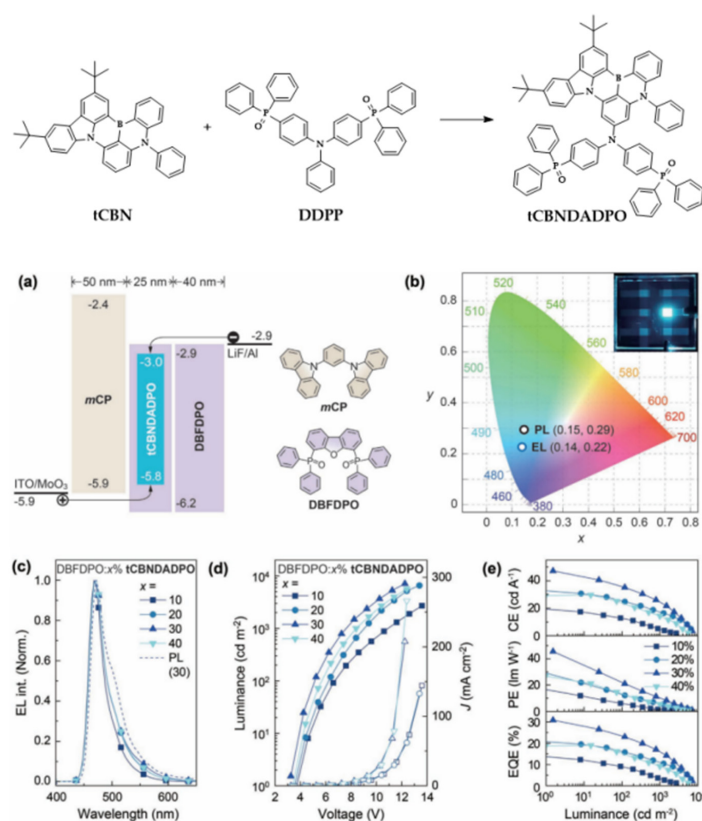
Unlike the continuous enhancement in their efficiency, the color purity of blue TADF emitters has barely been improved due to their broad emission spectrum caused by a large Stokes shift, which is a result of the twisted conformation of the D-A molecules and the structural relaxation in the excited states. Alternatively, TADF can also be achieved in molecules with an MR effect, such as P- and B-doped rigid polycyclic aromatic hydrocarbons (PAHs) [31–33], from which narrowband emission with high color purity can be achieved due to the suppressed structural relaxation and lower vibronic coupling between the  $S_1$ - $S_0$  transition and the stretching/scissoring vibrations. Since the first MR-TADF material was reported by Hatakeyama and co-workers in 2016 [31], significant progress has been made in terms of efficiency and color purity [34]. Typically, OLEDs with the blue MR-TADF emitter  $\nu$ -DABNA have demonstrated an emission maximum at 469 nm with an FWHM of 18 nm and an EQE<sub>max</sub> of 34.4% [35]. In addition, owing to their small Stokes shift, MR-TADF materials have been widely used as terminal emitters in hyper-fluorescent OLEDs to improve the color purity of devices with phosphorescent or TADF emitters only [36–40]. Nonetheless, pronounced efficiency roll-off, severe quenching at high concentrations, and limited device stabilities remain formidable challenges to developing efficient blue MR-TADF emitters. In this section, we focus on the reports that are likely to address these issues.

The efficiency roll-off of OLEDs based on MR-TADF emitters is usually severe when compared to devices with conventional TADF emitters, due to the longer decay lifetime of the former. The long decay lifetime of MR-TADF emitters is mainly caused by their moderate  $\Delta E_{ST}$  and RISC rate constant, which leads to an increased triplet-involved annihilation process [41–44]. Cao, Yang and colleagues presented a series of narrowband deep blue MR-TADF emitters (BN1–BN3, Figure 1) possessing a gradually enlarged ring-fused structure, which could simultaneously reduce  $\Delta E_{ST}$ , enhance  $f_{osc}$ , and retain narrow linewidth of MR-TADF emitters [45,46]. By measuring the threshold energy of low-temperature fluorescence and phosphorescence spectra, the  $\Delta E_{ST}$ s of BN1, BN2, and BN3 were deduced to be 0.20, 0.16, and 0.15 eV, along with gradually accelerated RISC rates of 1.3, 2.6, and  $25.5 \times 10^4 \text{ s}^{-1}$  at room temperature. Together with the shorter lifetime (17.8  $\mu\text{s}$ ) of the delayed fluorescent and a higher PLQY of 0.98 in DBFPO thin film, BN3 displayed improved EL performance in hyper-fluorescent OLEDs with a structure of ITO/HAT-CN (5 nm)/TAPC (30 nm)/TCTA(15 nm)/mCBP (10 nm)/DBFPO: 25 wt% 3Cz2BN: 1 wt% BN1–BN3 (25 nm)/DBFPO (15 nm)/ANT-BIZ (30 nm)/Liq/Al. In these devices, BN1–BN3 were used as terminal emitters, while 3Cz2BN was used as a TADF sensitizer. The high EQE<sub>max</sub> of 37.6% and EQE<sub>1000</sub> of 26.2%, as well as the deep blue color with CIE coordinates of (0.14, 0.08) of the device with BN1, indicated that chromophore  $\pi$ -extension could decrease the decay lifetime of MR-TADF emitters without weakening its PLQY and broadening its FWHM, and may eventually address the efficiency roll-off issue.



**Figure 1.** Molecular structures of BN1–BN3. (a) Device architecture for MR-TADF OLEDs with energy level alignment of the relevant material, (b) EL spectra, with CIE coordinates shown in the inset, (c) J–V–L characteristics, and (d) EQE–luminance curves of MR-TADF OLEDs. Reproduced with permission from Xialei Lv, Jingsheng Miao, Meihui Liu et al., “Extending the  $\pi$ -Skeleton of Multi-Resonance TADF Materials towards High-Efficiency Narrowband Deep-Blue Emission”; published by *John Wiley and Sons*, 2022. [45].

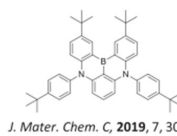
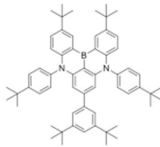
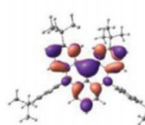
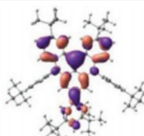
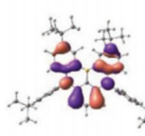
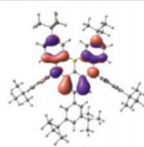
For most MR-TADF molecules, the functional groups are mostly simple, rigid, and finitely extended to avoid spectral broadening. Such highly planar configurations may lead to intermolecular interaction-induced quenching, such as triplet–triplet annihilation (TTA) and triplet–polaron quenching (TPQ), at high dopant concentrations. Thus, extremely low dopant concentrations (usually less than 5 wt%) of MR-TADF emitters are used in OLEDs, which may lead to a relatively low maximum luminance and substantial efficiency roll-off at high luminance. To address this issue, host-featured segments have been introduced to form self-host MR-TADF emitters. In addition to averting intermolecular interactions, transporting abilities can also be readily tuned in such self-host emitters [44,47,48]. As shown in Figure 2, Xu and co-workers reported an ambipolar self-host featured MR-TADF emitter, tCBNDADPO, in which a B–N framework (tCBN) was substituted with an ambipolar A–D–A host segment (DADPO). The D–A type PO structures of DADPO significantly improved the TADF properties of tCBNDADPO, especially the accelerated singlet radiative rate constant of  $2.11 \times 10^8 \text{ s}^{-1}$ , and exponentially reduced nonradiative rate constants, leading to a high PLQY of 99% for thin films with a high doping concentration of 30%. At the same time, narrowband blue emission with an FWHM of  $\approx 28 \text{ nm}$  was preserved in such film conditions. Taking advantage of the self-host feature, high EL performance of tCBNDADPO can be achieved in the OLED with a rather simple device structure of ITO/MoO<sub>3</sub> (6 nm)/mCP (50 nm)/tCBNDADPO: DBFDPO (25 nm)/DBFDPO (40 nm)/LiF (1 nm)/Al (100 nm). A high EQE<sub>max</sub> of 30.8% with coordinates of (0.14, 0.22) was achieved at a high concentration of 30%. Despite the efficiency roll-off (34.7% at a luminance of 300  $\text{cd m}^{-2}$ ) still being unsatisfactory, the high concentration tolerance and the simplified device structure utilized may pave a path to the practical application of self-host MR-TADF emitters.



**Figure 2.** Host–guest integration strategy for constructing tCBNDADPO to combine high color purity and efficiency. (a) Energy level diagram of devices and chemical structures of host and carrier transporting materials; (b) CIE coordinates of PL and EL emissions from DBFDPO:30% tCBNDADPO and device photo at 5 V; (c) concentration dependence of EL spectra and comparison to PL spectrum of 30% doped film; (d) variation of current density ( $J$ , hollow symbols)–voltage–luminance (solid symbols) characteristics at different  $x\%$ ; (e) dependence of efficiency versus luminance curves on  $x\%$ . Reproduced with permission from Jinkun Bian, Su Chen, Lili Qiu et al., “Ambipolar Self-Host Functionalization Accelerates Blue Multi-Resonance Thermally Activated Delayed Fluorescence with Internal Quantum Efficiency of 100%”; published by *John Wiley and Sons*, 2022 [44].

In addition to the serious efficiency roll-off, the relatively larger  $\Delta E_{ST}$  and lower RISC process of MR-TADF emitters also make it difficult to control the triplet exciton density in the device, leading to a short device lifetime. To address this issue, Park and colleagues demonstrated that by the introduction of an additional blocking group to manage intermolecular interaction and the concentration quenching effect, a high efficiency and stable MR-TADF OLED is possible [49]. With an additional di-tert-butylphenyl (dtB) substituent on 2,12-di-tert-butyl-5,9-bis(4-(tert-butyl)phenyl)-5,9-dihydro-5,9-diaza-13b-boranaphtho[3,2,1-de]anthracene (t-DABNA) [50], 2,12-di-tert-butyl-5,9-bis(4-(tert-butyl)phenyl)-7-(3,5-di-tert-butylphenyl)-5,9-dihydro-5,9-diaza-13b-boranaphtho[3,2,1-de]anthracene (t-DABNA-dtB) was synthesized, as shown in Figure 3. With the increase in doping concentration in mCBP films, the PLQY of t-DABNA gradually decreased from 87% at 3 wt% to 54% at 10 wt%. At the same doping concentrations, the PLQYs of t-DABNA-dtB were 97 and 78%, respectively. The high PLQY of t-DABNA-dtB at high concentrations is attributable to its larger HOMO–LUMO overlap and suppressed concentration quenching, which is a result of the bulky substituent. By using t-DABNA or t-DABNA-dtB as the emitting dopant in OLEDs with an architecture of ITO/BCFN:HATCN (40 nm, 30 wt%)/BCFN (10 nm)/mCBP (10 nm)/mCBP:mCBP-CN:Emitter (30 nm, 3 wt%)/DBFTRz (5 nm)/ZADN (20 nm)/LiF (1.5 nm)/Al (200 nm), high EQE<sub>max</sub> of over 25% were achieved. To further improve the device performance, especially the operational lifetime and efficiency roll-off, a sophisticated tandem device structure was adopted. High EQE<sub>max</sub> of 30.1%, which slightly decreased to 28.8% at high luminance of 1000 cd m<sup>-2</sup>,

was achieved in the tandem device with t-DABNA-dtB, together with a pure blue emission color with CIE coordinates of (0.116, 0.116) at 10,000  $\text{cd m}^{-2}$ . As shown in Figure 4, a long device lifetime,  $\text{LT}_{95}$ , of 502 h at an initial luminance of 1000  $\text{cd m}^{-2}$  was achieved in the tandem device. This lifetime is one of the best results for blue OLED lifetimes as reported in the literature, showing a bright future for blue MR-TADF in practical applications.

	t-DABNA	t-DABNA-dtB
<b>Molecular Structure</b>	 <i>J. Mater. Chem. C, 2019, 7, 3082</i>	
<b>LUMO (eV)</b>	 -0.78	 -1.09
<b>HOMO (eV)</b>	 -4.58	 -4.59
<b>f (<math>S_0-S_1</math>)</b>	0.2335	0.2290
<b><math>E_{\text{gap}}</math> (eV)</b>	3.61	3.51

**Figure 3.** Molecular structures and DFT calculations of t-DABNA and t-DABNA-dtB. Reproduced with permission from Jinho Park, Ki Ju Kim, Junseop Lim et al., “High Efficiency of over 25% and Long Device Lifetime of over 500 h at 1000 nit in Blue Fluorescent Organic Light-Emitting Diodes”; published by *John Wiley and Sons*, 2022 [49].

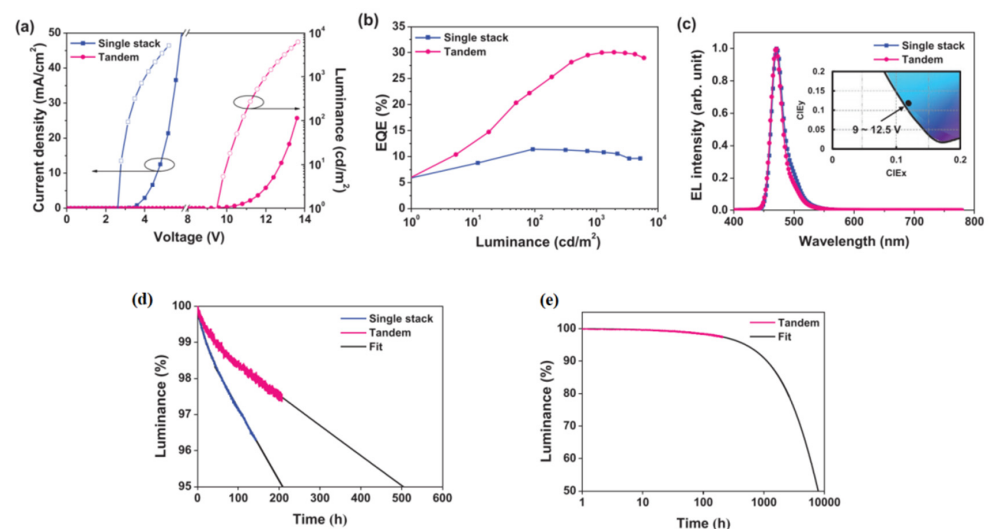


**Figure 4.** (a) J–V–L and (b) EQE–L characteristics, (c) EL spectra and CIE coordinates (inset), and (d) lifetime data of single stack and tandem devices. (e) Extrapolated plot of the tandem device. Reproduced with permission from Jinho Park, Ki Ju Kim, Junseop Lim et al., “High Efficiency of over 25% and Long Device Lifetime of over 500 h at 1000 nit in Blue Fluorescent Organic Light-Emitting Diodes”; published by *John Wiley and Sons*, 2022 [49].

### 3. Blue TSCT-TADF Emitters

In addition to emitters in a twisted D- $\pi$ -A structure via through-bond charge transfer (TBCT), TADF can also be the result of TSCT processes that usually take place between a pair of exciplex-forming D and A molecules, which is known as inter-TSCT. On the other hand, TSCT-TADF emitters (intra-TSCT) are molecules where the D and A segments are linked in a V or U shape, in which TSCT between D and A segments is possible. When compared with TBCT emitters, TSCT emitters have reduced electronic communication and coupling between D and A moieties, which benefits the elevation of the singlet and triplet levels and thus blue emission. At the same time, high PLQYs could easily be achieved in the TSCT molecules with intrinsic intramolecular noncovalent interactions [51,52]. The distance and orientation between D and A segments, determined by the linker, is a crucial factor in the excited state dynamics of a TSCT-TADF emitter [53]. Of the various types of alignment of D and A segments in TSCT molecules, face-to-face alignment with short distance is the most favorable for efficient TADF emission. However, only a few blue examples have been reported among high-performance OLEDs with TSCT-TADF emitters [54–60].

As shown in Figure 5, Wang and co-workers demonstrated a TADF polymer in which the TSCT effect takes place between pendant D and A units on a nonconjugated polyethylene backbone [59]. Unlike conventional conjugated D-A polymers, there is no direct conjugation between D and A units in the TSCT-TADF polymer because of its nonconjugated architecture, which is favorable for blue emission. Two polymers with the same A unit of 2,4,6-triphenyl-1,3,5-triazine (TRZ) but different D units of 9,9-dimethyl-10-phenyl-acridan (Ac) or 9,9-bis(1,3-ditert-butylphenyl)-10-phenyl-acridan (TBAC) were synthesized and compared. As a result of its steric 1,3-ditert-butylphenyl groups, the acridan unit is separated from the triazine unit in the TBAC-based polymer, while acridan approaches triazine in the Ac-based polymer, which determines the different D-A distance in different polymers. As expected, since TSCT is highly sensitive to the D-A distance, the distinct TSCT effect and TADF feature were only displayed in the Ac-based polymer, where a small  $\Delta E_{ST}$  of 0.019 eV and high PLQY up to 60% in the film state were achieved. On the other hand, no TSCT effect and only fluorescence emission were found in the TBAC-based counterpart. When the polymer with 95 mol % Ac and 5 mol % TRZ (P-Ac95-TRZ05) was used as the EML in the device with a structure of ITO/PEDOT: PSS (40 nm)/P-Ac95-TRZ05 (40 nm)/TSPO1 (8 nm)/TmPyPB(42 nm)/LiF (1 nm)/Al (100 nm), blue emission with CIE coordinates of (0.176, 0.269) and an  $\text{EQE}_{\text{max}}$  of 12.1% were achieved, which is the first example of blue TSCT-TADF polymer for solution-processed OLEDs.

Zhang, Duan and colleagues adopted a xanthene bridge to construct space-confined face-to-face D-A alignment and minimize the D-A distance to 2.7–2.8 Å to strengthen the electronic interaction between weak D and A, which is required for efficient blue emission [39]. The targeted TSCT-TADF emitters are shown in Figure 6, exhibiting peaks around 460 nm, PLQYs > 90%, and a  $k_{\text{rs}}$  of nearly  $107 \text{ s}^{-1}$ . The EL of such blue emitters was investigated in OLEDs with a structure of ITO/HAT-CN (5 nm)/TAPC (30 nm)/TCTA (10 nm)/mCP (10 nm)/PPF: 30 wt% emitters (24 nm)/PPF (10 nm)/BPhen (30 nm)/LiF (0.5 nm)/Al (150 nm). Blue emission with an  $\text{EQE}_{\text{max}}$  of 27.8% and CIE coordinate of (0.17, 0.29) were achieved when dCz-Xo-TRZ was used as the emitter. dCz-Xo-TRZ was further used as a sensitizer in hyper-fluorescent OLEDs with the well-known MR-TADF emitter, *v*-DABNA, as the terminal emitter. A high  $\text{EQE}_{\text{max}}$  of 34.7% with a  $\text{CIE}_y$  coordinate of 0.15 and FWHM of 19 nm was realized in the resulting device.

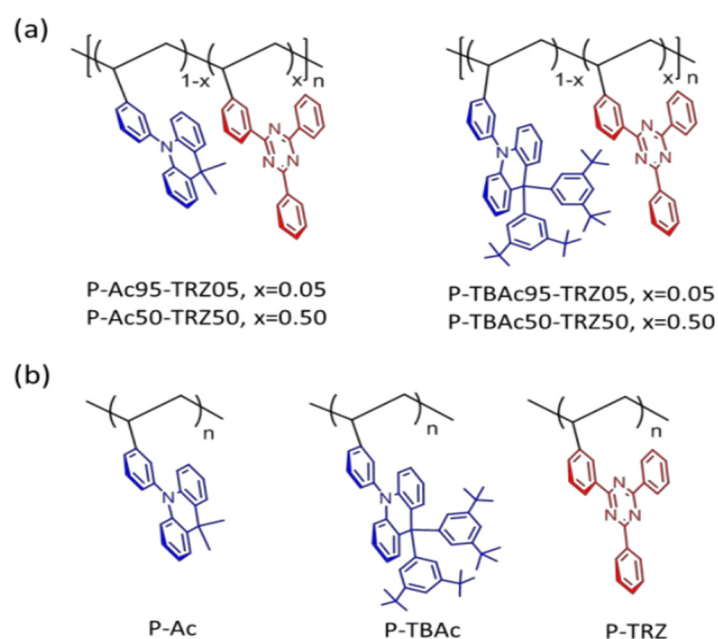


**Figure 5.** Molecular structures of (a) TSCT-based polymers and (b) the corresponding control polymers. Reprinted with permission from Shao, S.; Hu, J.; Wang, X.; Wang, L.; Jing, X.; Wang, F. “Blue Thermally Activated Delayed Fluorescence Polymers with Nonconjugated Backbone and Through-Space Charge Transfer Effect” [J]. *J. Am. Chem. Soc.* **2017**, *139*, 17739–17742. Copyright 2017 American Chemical Society [59].

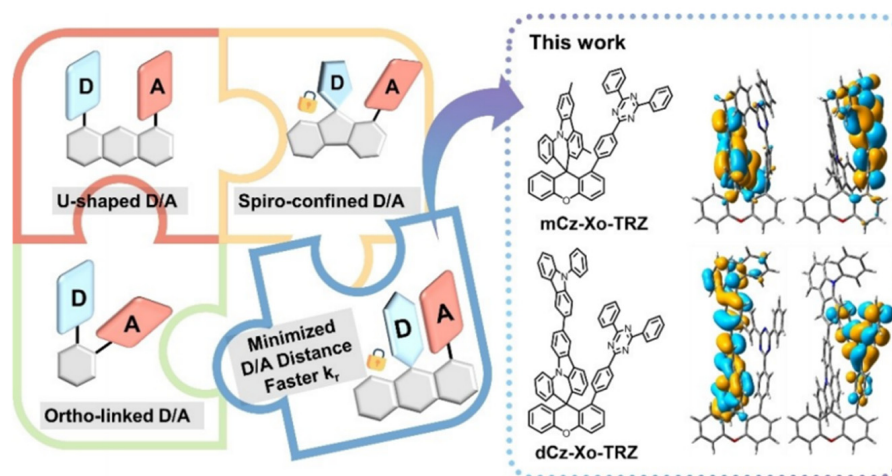


**Figure 6.** TSCT-TADF molecules with different types of donor–acceptor alignments, and molecular structures of mCz-Xo-TRZ and dCz-Xo-TRZ with their HOMO/LUMO distribution. Reproduced with permission from Tianyu Huang, Qi Wang, Guoyun Meng et al., “Accelerating Radiative Decay in Blue Through-Space Charge Transfer Emitters by Minimizing the Face-to-Face Donor–Acceptor Distances”; published by *John Wiley and Sons*, **2022** [39].

Despite the high efficiency achieved in blue TSCT-TADF emitters [39,55,57], their color purity is still far from meeting the ultrapure-blue requirements of CIE (0.14, 0.08) defined by the NTSC, as well as CIE (0.131, 0.046) for the standard of Rec. 2020 [60], due to the large Stokes shift and broad emission with large FWHM in conventional TADF emitters. Alternatively, as mentioned in Section 2, the FWHM can be effectively narrowed by using MR-TADF emitters due to their rigid polycyclic aromatic framework. Ren and co-workers designed TSCT-TADF emitters by combining acridine derivatives and electron-withdrawing boron/oxygen heterocycles [60]. As depicted in Figure 7, by controlling the intramolecular stacking of rigid heteroaromatic compounds, deep blue emission with a

narrow FWHM could be achieved. By using AC-BO, QAC-BO, and Cz-BO as emitters in OLEDs with a structure of ITO/HAT-CN (20 nm)/TAPC (40 nm)/mCP (10 nm)/20% emitters: DPEPO (20 nm)/DPEPO (10 nm)/TmPyPB(50 nm)/LiF (1 nm)/Al (150 nm), the EL properties of AC-BO, QAC-BO, and Cz-BO were investigated. With decreasing stacking distance, emission maxima of AC-BO, QAC-BO, and Cz-BO were significantly blue-shifted from 456 to 412 nm, while the FWHM narrowed from 71 to 43 nm, leading to CIE coordinates of (0.147, 0.122), (0.145, 0.076), and (0.163, 0.034), respectively. The device with AC-BO shows an  $\text{EQE}_{\text{max}}$  of 19.3%, the best performance among all deep blue TSCT-TADF emitters so far [60]. The device with QAC-BO achieved an  $\text{EQE}_{\text{max}}$  of 15.8%, making it the first high-efficiency TSCT-TADF material to meet the ultrapure blue requirements of CIE (0.14, 0.08) defined by the NTSC. Nonetheless, the relatively low maximum luminance of less than  $1000 \text{ cd m}^{-2}$  and pronounced efficiency roll-off of more than 60% at  $100 \text{ cd m}^{-2}$  hinders the practical application of these deep blue emitters.

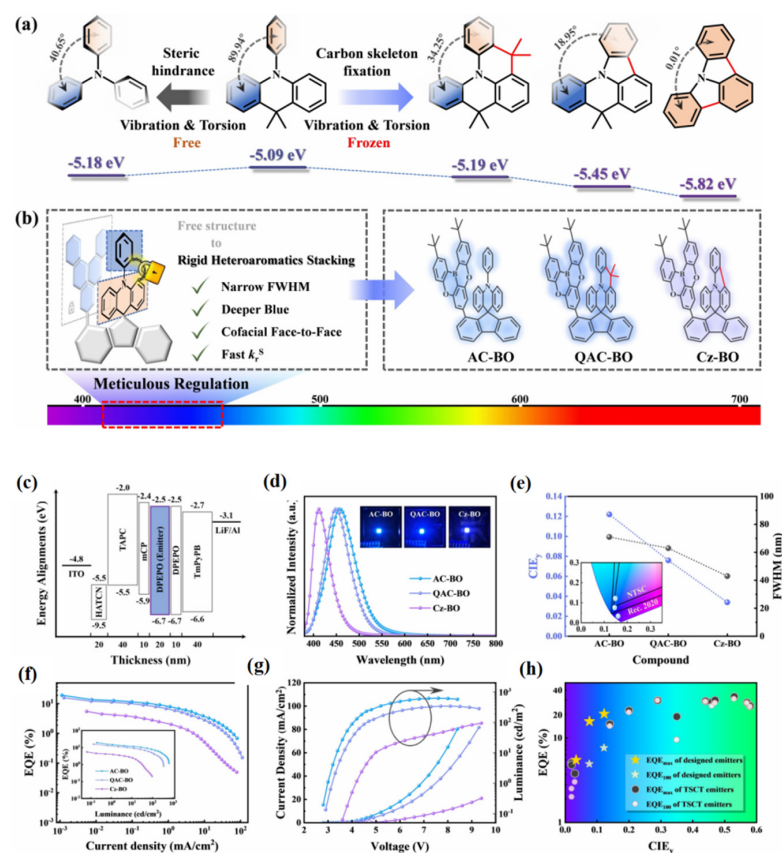


**Figure 7.** (a) The relationship between structures and HOMO levels of phenyl acridine and its skeleton-modified derivatives based on the DFT simulations. (b) Design strategy for controlling intramolecular stacking of rigid heteroaromatic compounds and the chemical structures of the designed compounds. (c) Device configuration and the related energy levels. (d) EL spectra with the photographs of devices (inset). (e) CIE<sub>y</sub> and FWHM of the EL spectra with CIE plot of EL spectra (inset). (f) EQE–current density curves with EQE–luminance curves (inset). (g) Current density–voltage–luminance curves. (h) EQE<sub>max</sub> and EQEs at  $100 \text{ cd m}^{-2}$  (EQE<sub>100</sub>) of this work and the reported TSCT emitters. Reproduced with permission from Zhennan Zhao, Cheng Zeng, Xiaomei Peng et al., “Tuning Intramolecular Stacking of Rigid Heteroaromatic Compounds for High-Efficiency Deep-Blue Through-Space Charge-Transfer Emission”; published by *John Wiley and Sons*, 2022 [60].

#### 4. Blue Metal-TADF Emitters

Despite their rapid development, the long-term stability of OLEDs with organic TADF emitters is still inferior when compared with those with phosphorescent or fluorescent emitters, due to the long-lived triplet excitons of organic TADF molecules resulting from

their inefficient spin–orbital coupling (SOC) [61,62]. Alternatively, by taking advantage of the strong SOC of phosphorescent organometallic complexes, metal-TADF emitters may achieve high emission quantum yields and fast radiative decay rates, and thereby eventually find practical applications in the OLED industry. Since Yersin and co-workers demonstrated the first TADF emission from a [(pop)Cu(N`N)] complex, in addition to Cu(I) emitters [63,64], second and third row transition metal complexes, such as those of Pd(II), Ag(I), Au(I), and Au(III), have been developed as TADF emitters [65,66]. Among the reported metal-TADF emitters, those based on two-coordinate carbene-metal-amide (CMA) emitters and tetradentate Au(III) complexes have displayed the best performance in terms of efficiency and stability [67,68]. Nonetheless, performances of blue-emitting OLEDs with metal-TADF were relatively inferior when compared to those of green, yellow, and red in terms of efficiency and color purity, until a recent publication presented blue-emitting metal-TADF emitters based on Cu(I) and Au(I) complexes [40,62,65,66,69–72].

As shown in Figure 8, by substituting  $\text{CF}_3$  and  $^t\text{Bu}$  for the carbazole substitution of the CMA(Au) emitter they reported earlier [67], Romanov, Credginton and colleagues developed a highly efficient blue-emitting metal-TADF emitter Au(I)-1 [71]. Since the HOMO is almost entirely located on the Cz donor of the ( $^{\text{Ad}}$ CAAC)AuCz archetype, the introduction of electron-withdrawing groups to this moiety influences the HOMO more than the LUMO. It widens the HOMO–LUMO gap, shifting it towards blue emission [67]. A high quantum yield of 0.96 with an emission maximum located at 495 nm was achieved in Au(I)-1 in toluene solution. Considering that the high polarity of CMA compounds makes their emission energies sensitive to their molecular environment, allowing the “tuning” of EL by suitable host media from green to sky blue, the emission maximum of Au(I)-1 can be tuned from 484 nm in neat film to 479 and 464 nm when doped in o-CBP and DPEPO hosts, respectively. The EL performance of Au(I)-1 was characterized by an OLED with a device structure of ITO/TAPC (40 nm)/o-CBP (5 nm)/EML (30 nm)/TSPO1 (40 nm)/LiF (1 nm)/Al (100 nm). In addition, since CMAs do not suffer from strong concentration quenching in the solid state, attributed to the lack of close metal–metal contacts, host-free OLEDs with neat Au(I)-1 as the EML have also been fabricated. Similar to the trend in the PL spectra, the device with the high-polarity DPEPO host shows the best color purity, with a maximum located at 450 nm, leading to CIE coordinates of (0.17, 0.17) along with a high EQE of up to 20.9%. Encouragingly, a high performance with an EQE of up to 17.3% and CIE coordinates of (0.18, 0.27) were also achieved in the host-free Au(I)-1-based OLED.

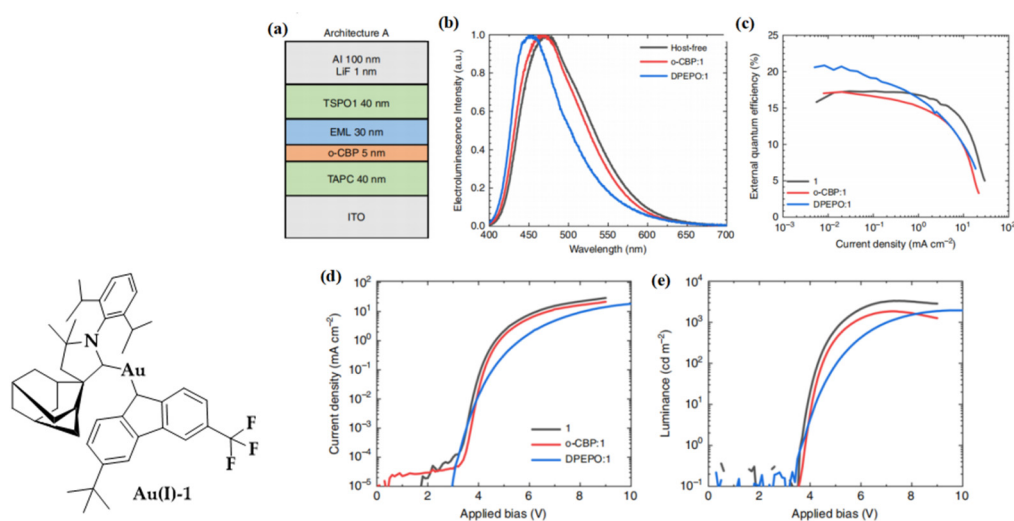


**Figure 8.** Molecular structure of Au(I)-1. (a) Schematic OLED architecture used; (b) normalized EL spectra, (c) EQE–current density, (d) current–voltage, and (e) luminance–voltage characteristics of OLEDs with Au(I)-1 in host-free and host-guest structures. Reproduced with permission from Patrick J. Conaghan et al., “Highly efficient blue organic light-emitting diodes based on carbene-metal-amides”; published by *Springer Nature*, 2020 [71].

As depicted in Figure 9, by modifying **a5**, whose HOMO and LUMO are localized on the aryl donor triphenylamine (TPA) and mainly on the C<sup>∞</sup>N<sup>∞</sup>C ligand [73], respectively, two blue-emitting Au(III)-TADF complexes were developed by lowering the HOMO energy or raising the LUMO energy. Specifically, Au(III)-1 was prepared by replacing the OEt group in complex **a5** with a more electron-donating dimethyl-amine group to raise the LUMO energy, while Au(III)-2 was prepared by further substituting the phenyl rings of the TPA with electron-withdrawing F substituents to lower the HOMO energy. By means of electrochemistry, the LUMO energy of Au(III)-1 and Au(III)-2 was measured to be 0.18 eV higher than that of complex **a5**, attributable to the replacement of the OEt group by the more electron-donating NMe<sub>2</sub> group. For Au(III)-2, the fluorine substituents on the TPA ligand slightly lowered the HOMO energy by about 0.03 eV from that of Au(III)-1. Thus, PL maxima at 484 and 470 nm were achieved in Au(III)-1 and Au(III)-2, respectively, in PMMA thin film. Despite its less blue emission, the high PLQY of 0.82 for Au(III)-1 in PMMA thin film is much higher than that (0.34) of Au(III)-2. By their application in solution-processed OLEDs, EL properties of both TADF Au(III) complexes were investigated. The device structure was ITO/PEDOT:PSS/OTPD (4 nm)/PYD2: Au-emitter (60 nm)/DPEPO (10 nm)/TPBi (40 nm)/LiF (1.2 nm)/Al (100 nm). The Au(III)-1- and Au(III)-2-based devices show EL maxima at 473 and 465 nm, respectively, with a FWHM of 64–67 nm and CIE coordinates of (0.16, 0.25) for the former and (0.16, 0.23) for the latter. Due to its higher PLQY, the EQE<sub>max</sub> of 15.25% shown by the Au(III)-1-based device is much higher than that of the Au(III)-2-based device (6.76%). By employing an MR-TADF blue emitter, v-DABNA, as the terminal emitter, a hyper-fluorescent solution-processed OLED was fabricated using the same device structure for Au(III)-1 (Figure 10). Efficient ET from Au(III)-1 to v-DABNA, with an estimated Förster distance of 2.83 nm and an ET rate of  $2.35 \times 10^7 \text{ s}^{-1}$ , was determined by photophysical investigations. The blue hyper-fluorescent OLED achieved a high EQE<sub>max</sub> of 16.6%, a narrowband emission with an FWHM of 23 nm, and high color purity with CIE coordinates of (0.14, 0.18). When compared with that (30%) of the Au(III)-1 only device, the efficiency roll-off (13%) of the hyper-fluorescent device was significantly improved, attributable to the effective ET process in the latter that could lower the population of triplet excitons in Au(III)-1 at high luminance [40].

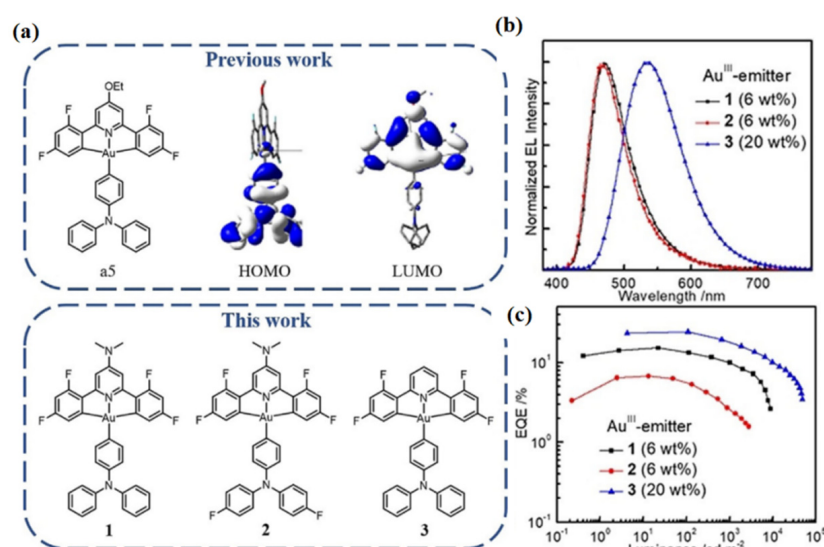


**Figure 9.** (a) Top: previously reported arylgold(III)-TADF complex **a5** and its HOMO and LUMO surfaces. Bottom: donor–acceptor type C<sup>∞</sup>N<sup>∞</sup>C gold(III) complexes Au(III)-1–Au(III)-3 in this work; (b) normalized EL spectra; and (c) EQE–luminance characteristics of OLEDs based on Au(III)-1, Au(III)-2, and Au(III)-3 at their optimized doping concentration. Reproduced with permission from Dongling Zhou, Gang Cheng, Glenna So Ming Tong et al., “High Efficiency Sky-Blue Gold(III)-TADF Emitters”; published by *John Wiley and Sons*, 2020 [72].

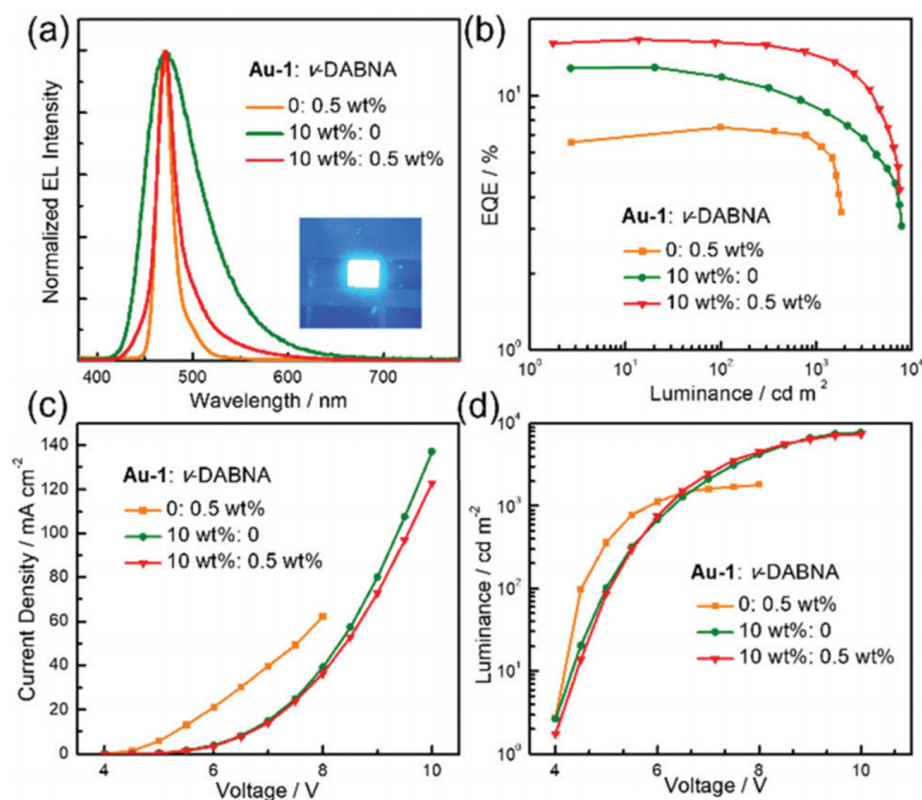


**Figure 10.** (a) Normalized EL spectra, (b) EQE–luminance, (c) current density–voltage, and (d) luminance–voltage characteristics of OLEDs with different concentrations of Au(III)-1 and  $\nu$ -DABNA. The image of the sensitized OLED is shown in the inset of (a). Reproduced from Ref. [40] with permission from the Royal Society of Chemistry.

Since the reports of CMA emitters based on bulky NHC ligands, with emission quantum yields up to unity, a  $k_r$  of up to  $1 \times 10^6 \text{ s}^{-1}$ , and EL efficiency up to 20%, Cu(I) complexes have been expected to replace expensive phosphorescent complexes in OLEDs as emitters [64,67,70,74]. Nonetheless, the operational stability of Cu(I)-based OLEDs, especially that of blue-emitting ones, has barely been reported in the literature [75]. With the use of heterocyclic  $\pi$ -annulated NHC ligands with appreciable  $\pi$ -acidity, we report a panel of thermally and air-stable CMA(Cu)-TADF emitters based on bulky pyrazine- and pyridine-fused NHC ligands [62]. As a blue-emitter, Cu-5 (Figure 11) shows PL emission with a maximum at 470 nm, a PLQY of 0.52, and a  $k_r$  of  $1.1 \times 10^6 \text{ s}^{-1}$  in thin films. EL performance of Cu-5 was investigated in a vacuum-deposited OLED with a device structure of ITO/HAT-CN (5 nm)/TAPC (50 nm)/TCTA (10 nm)/Cu-5: TCTA: DPEPO (20 nm)/DPEPO (10 nm)/TPBi (40 nm)/LiF (1 nm)/Al (100 nm). When the doping concentration was 4 wt%, the Cu5-based device displayed a blue emission with an EL maximum located at 474 nm and CIE coordinates of (0.14, 0.22), as well as a high  $\text{EQE}_{\text{max}}$  of 23.6%, which is among the best blue OLEDs reported in the literature [76,77]. Notably, the operational lifetime ( $\text{LT}_{90}$ ) of OLEDs based on Cu5 was 0.4 h at an  $L_0$  of  $7600 \text{ cd m}^{-2}$ , corresponding to 11.6 h at an  $L_0$  of  $1000 \text{ cd m}^{-2}$  using the acceleration coefficient ( $n$ ), obtained as shown in Figure 11. By using  $\nu$ -DABNA as a terminal emitter, hyper-fluorescent OLEDs with Cu5 as a sensitizer showed an improved color purity with CIE coordinates of (0.15, 0.20) and a longer  $\text{LT}_{90}$  of 12.2 h at an  $L_0$  of  $1000 \text{ cd m}^{-2}$ .

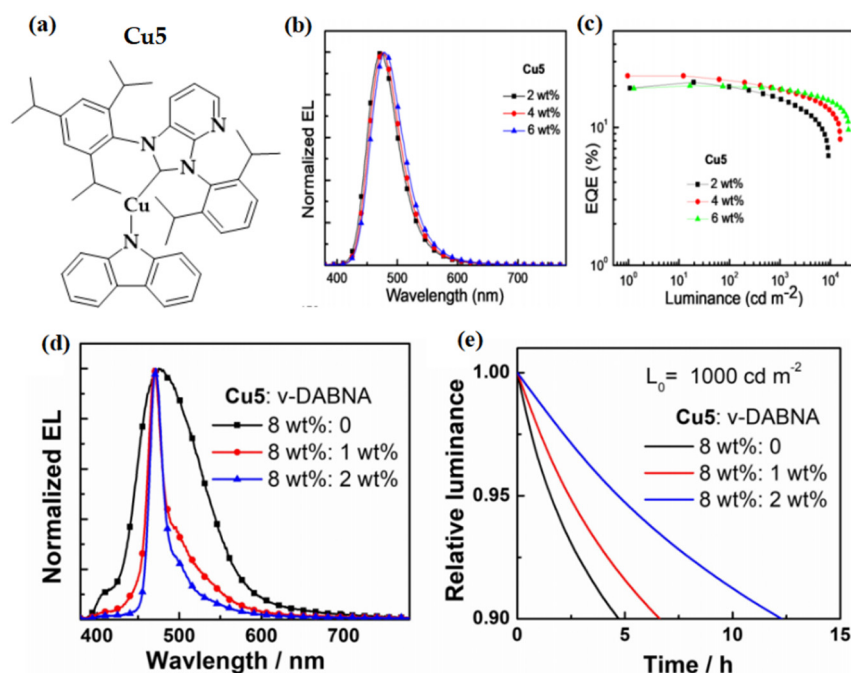


**Figure 11.** (a) Molecular structure of Cu5; (b) normalized EL spectra; (c) EQE–luminance of OLEDs based on Cu5 with various doping concentrations ranging from 2 to 6 wt%; (d) EL spectra; and (e) relative luminance versus operation time at an  $L_0$  of  $1000 \text{ cd m}^{-2}$  of the hyper-OLEDs with Cu5 and v-DABNA. Reproduced with permission from Rui Tang, Shuo Xu, Tsz-Lung Lam et al., “Highly Robust CuI-TADF Emitters for Vacuum-Deposited OLEDs with Luminance up to  $222,200 \text{ cd m}^{-2}$  and Device Lifetimes (LT90) up to 1300 hours at an Initial Luminance of  $1000 \text{ cd m}^{-2}$ ”; published by *John Wiley and Sons*, 2022 [62].

## 5. Outlook and Perspective

Bimolecular annihilations, such as TTA and TPA, caused by the long decay time of TADF emitters are the main reason for the efficiency roll-off and unsatisfactory stability of TADF-OLEDs, particularly blue ones. To surmount such disadvantages, specific molecular structures with extremely small or even negative  $\Delta E_{ST}$  have been designed to decrease the decay time [78–82].

Yersin and co-workers reported a strategy to design a new type of emitter based on a new exciton harvesting mechanism by significantly reducing  $\Delta E_{ST}$ , rigidifying molecular structure, maximizing the Franck–Condon factors, shifting the charge transfer states, and providing energetically nearby lying states [78]. As shown in Figure 12, in the designed compound DSH, both D and A moieties are rigidly linked by two bridges at relatively large separations [81]. Thus, the low-lying CT states,  $^1\text{CT}(\text{DA})$  and  $^3\text{CT}(\text{DA})$ , have a minimal splitting of  $\approx 10 \text{ cm}^{-1}$  (1.2 meV), while the fluorene-substituted bridge can further stabilize the molecular structure. At the same time, one more low-lying fluorene-localized  $^3\text{LE}(\text{F})$  state is found in the fluorene-substituted bridge. Their design mitigated the forbidden ISC processes, enabling faster ISC and RISC rates for DSH than those of conventional TADF emitters. Thus, the long decay times of conventional TADF emitters can be avoided in DSH. By using DSH as an emitting dopant in OLEDs, with a structure of ITO/HAT-CN (5 nm)/TAPC (40 nm)/CCP (10 nm)/DSH: PPF (10 nm)/PPF (10 nm)/Tm3PyBPZ (40 nm)/LiF (1.2 nm)/Al (100 nm), an  $\text{EQE}_{\text{max}}$  of 18.7% with an EL maximum at 486 nm was achieved. Although the device performance and emission color are strongly dependent on the dielectric constant of the host material, which could cause difficulty in optimizing the device structure, the specific molecular design of DSH provides a guideline for next-generation TADF materials.

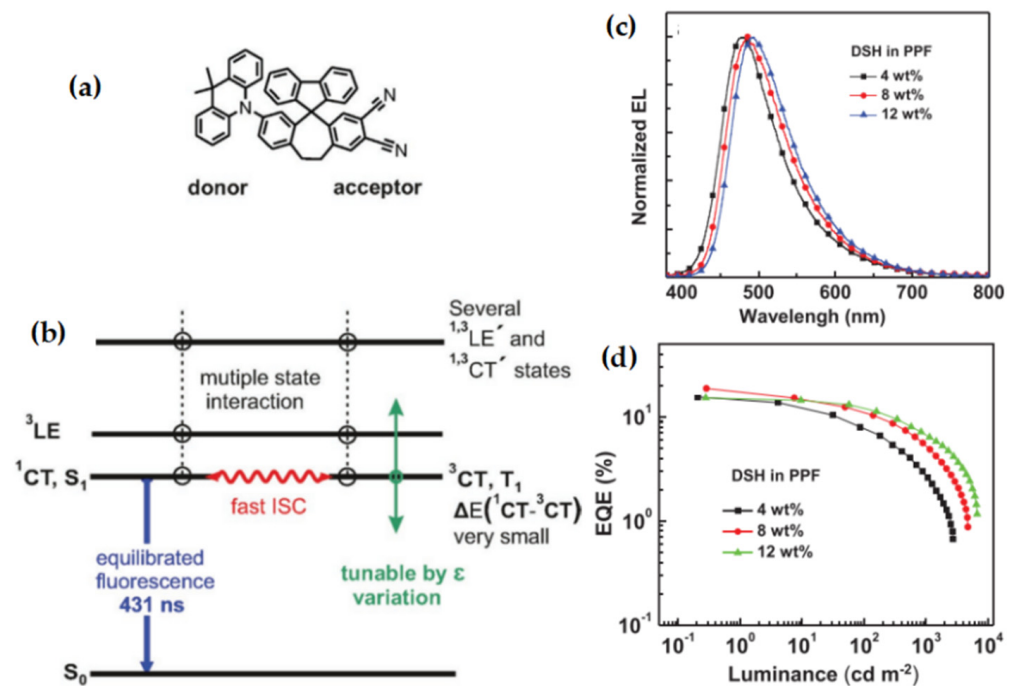


**Figure 12.** (a) Molecular structure of DSH; (b) simplified energy level diagram for the DSH molecule; (c) normalized EL spectra and (d) EQE–luminance characteristics of OLEDs with different concentrations of DSH. Reproduced with permission from Hartmut Yersin, Rafał Czerwieniec, Larisa Mataranga-Popa et al., “Eliminating the Reverse ISC Bottleneck of TADF Through Excited State Engineering and Environment-Tuning Toward State Resonance Leading to Mono-Exponential Sub- $\mu$ s Decay. High OLED External Quantum Efficiency Confirms Efficient Exciton Harvesting”; published by *John Wiley and Sons*, 2022 [81].

Despite the general agreement that  $\Delta E_{ST}$  must be positive, some nitrogen-substituted phenalene analogues have the potential for a negative  $\Delta E_{ST}$ , which can be attributed to the double-excitation configurations. Two electrons of occupied orbitals are promoted to virtual orbitals in double-excitation configurations [83–86]. Since the accessible double-excitation configurations in  $T_1$  are restricted (Pauli exclusion principle), an effective admixture of such configurations stabilizes  $S_1$ , leading to a possibly negative  $\Delta E_{ST}$  when the stabilization overcomes the exchange energy (Figure 13a). With the motivation of discovering molecules with negative  $\Delta E_{ST}$ , from which delayed fluorescence from inverted singlet and triplet (DFIST) excited states can be observed, Miyajima and colleagues computationally screened 34,596 molecules, which were heptazine analogues with 186 different substituents [82]. Among the screening results, HzTFEX<sub>2</sub> and HzPipX<sub>2</sub> (Figure 13b), were compared. Theory (EOM-CCSD) calculations revealed that HzTFEX<sub>2</sub> has a negative  $\Delta E_{ST}$  of  $-12$  meV, while HzPipX<sub>2</sub> has a small positive  $\Delta E_{ST}$  of 10 meV. Measurements of the photophysics and transient PL decay further confirmed the negative  $\Delta E_{ST}$  of HzTFEX<sub>2</sub>, which exhibits DFIST. When it was used as the emitting dopant in the device with a structure of Glass/ITO (130 nm)/PEDOT: PSS (30 nm)/MoO<sub>3</sub> (5 nm)/BST (3 nm)/DBFSiDBF (10 nm)/PPF: 10 wt% HzTFEX<sub>2</sub> (15 nm)/PPF (10 nm)/Alq<sub>3</sub> (40 nm)/Li<sub>q</sub> (1 nm)/Al (80 nm), intense blue EL originating from HzTFEX<sub>2</sub> was observed with an EQE<sub>max</sub> of 17% and EL maxima at 450 nm and 479 nm with CIE coordinates of (0.17, 0.24). The remarkable efficiency roll-off suggests that great efforts are still needed to fully exploit the benefits of negative  $\Delta E_{ST}$  in EL devices.

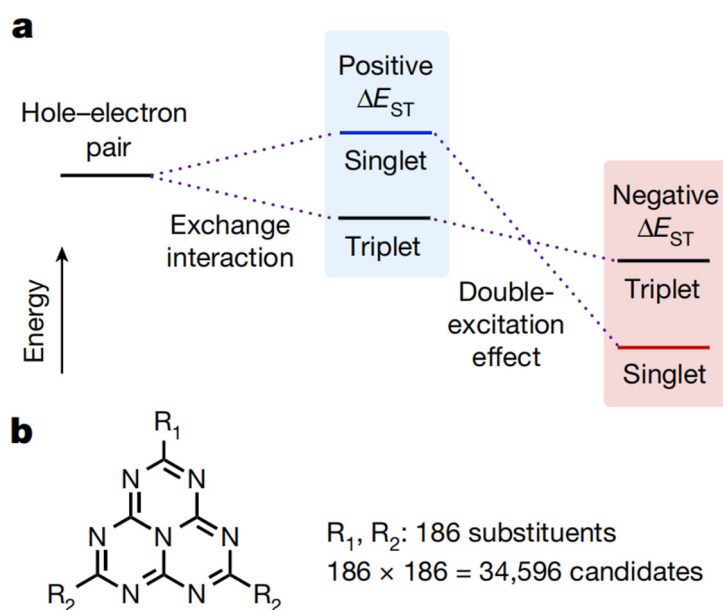


**Figure 13.** (a) Schematic diagram of singlet and triplet excited states split in energy by the exchange interaction (middle) and then inverted by including the double-excitation effect (right); (b) molecular structures of the heptazine analogues examined in the computational screening. Reproduced with permission from Naoya Aizawa et al., “Delayed fluorescence from inverted singlet and triplet excited states”; published by *Springer Nature*, 2022 [82].

**Author Contributions:** Conceptualization, Y.G. and S.W.; writing—original draft, Y.G. and S.W.; writing—review and editing, Y.G., G.S. and G.C.; supervision, G.C. All authors have read and agreed to the published version of the manuscript.

**Funding:** This work was financially supported by the Guangdong Major Project of Basic and Applied Basic Research (2019B030302009), Hong Kong Quantum AI Lab Limited, Innovation and Technology Fund (PRP/071/19FX), Shunde Science and Technology Bureau (2030218000158), and Science Technology and Innovation Commission of Shenzhen Municipality (JCYJ20180508162429786 and JCYJ20200109150414471).

**Data Availability Statement:** Not applicable.

**Conflicts of Interest:** The authors declare no conflict of interest.

## Appendix A

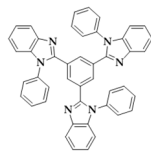
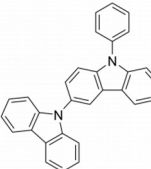
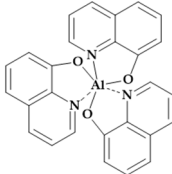
**Table A1.** Full name, molecular structure and function of auxiliary materials used in OLEDs in this review.

Material	Full Name	Structure	Function
HAT-CN	Dipyrazino[2,3-f:2',3'-h]quinoxaline-2,3,6,7,10,11-hexacarbonitrile		HIL
TAPC	Di-[4-(N,N-ditolyl-amino)-phenyl]cyclohexan		HTL

Table A1. Cont.

Material	Full Name	Structure	Function
TCTA	4,4',4''-Tris(carbazol-9-yl)-triphenylamine		HTL
mCBP	3,3-Di(9H-carbazol-9-yl)biphenyl		HTL
ANT-BIZ	1-(4-(10-([1,1'-biphenyl]-4-yl)anthracen-9-yl)phenyl)-2-ethyl-1H-benzo[d]imidazole		ETL
mCP	1,3-Di(9H-carbazol-9-yl) benzene, N,N'-Dicarbazolyl-3,5-benzene		HTL
BCFN	N-([1,1'-biphenyl]-4-yl)-9,9-dimethyl-N-(4-(9-phenyl-9H-carbazol-3-yl)phenyl)-9H-fluoren-2-amine		HTL
DBFTRz	2,8-Bis(4,6-diphenyl-1,3,5-triazin-2-yl)dibenzo[b,d]furan		HBL
ZADN	2-(4-(9,10-Di(naphthalen-2-yl)anthracen-2-yl)phenyl)-1-phenyl-1H-benzo[d]imidazole		ETL
TSPO1	Diphenyl[4-(triphenylsilyl)phenyl]phosphine oxide		HBL
TmPyPB	1,3,5-tri[(3-pyridyl)-phen-3-yl]benzene		ETL
PPF	2,8-Bis(diphenylphosphoryl)dibenzo[b,d]furan		HTL
BPhen	4,7-diphenyl-1,10-phenanthroline		HBL
OTPD	[N,N'-bis(4-(6-((3-ethyloxetan-3-yl)methoxy))-hexylphenyl)-N,N'-diphenyl-4,4'-diamine]		HIL
PYD2	2,6-Bis(9H-carbazol-9-yl)pyridine, 9,9-(2,6-pyridinediyl)bis-9H-carbazole		Host

Table A1. Cont.

Material	Full Name	Structure	Function
TPBi	2,2',2''-(1,3,5-benzinetriyl)-tris(1-phenyl-1-H-benzimidazole)		ETL
CCP	9-Phenyl-9H-3,9'-bicarbazole		HTL
Alq3	Tris(8-hydroxyquinolino)aluminium		ETL

## Appendix B

Table A2. Key performances of blue OLEDs described in this review and recent results.

Type	Emitter	EQE <sub>max</sub> <sup>a</sup> [%]	EQE <sub>1000</sub> <sup>b</sup> [%]	Lifetime [h]	λ <sub>max</sub> <sup>c</sup> [nm]	FWHM [nm]	CIE Coordinates [x, y]	Ref.
MR-TADF	v-DABNA	34.4	26.0	-	469	18	(0.12, 0.11)	[35]
	BN1	31.2	9.3	-	457	28	(0.14, 0.08)	[45]
	BN2	33.2	15.5	-	467	23	(0.13, 0.11)	[45]
	BN3	37.6	26.2	27.2 <sup>d</sup>	458	23	(0.14, 0.08)	[45]
	tCBNDADPO	30.8	16.2	-	472	28	(0.14, 0.22)	[44]
	t-DABNA	25.2	-	-	465	27	(0.126, 0.102)	[49]
	t-DABNA-dtB	30.1	28.8	502 <sup>e</sup>	471	22	(0.117, 0.112)	[49]
TSCT-TADF	P-Ac95-TRZ05	12.1	11.5	-	479	-	(0.176, 0.269)	[59]
	dCz-Xo-TRZ	27.8	23.9	-	477	19	(0.17, 0.29)	[39]
	AC-BO	19.3	-	-	456	71	(0.147, 0.122)	[60]
	QAC-BO	15.8	-	-	448	63	(0.145, 0.076)	[60]
	Cz-BO	5.5	-	-	412	43	(0.163, 0.034)	[60]
Metal-TADF	Au(I)-1	20.9	-	-	450	-	(0.17, 0.17)	[71]
	Au(III)-1	15.25	9.98	-	473	64	(0.16, 0.25)	[72]
	Au(III)-2	6.76	2.51	-	465	67	(0.16, 0.23)	[72]
	Cu5	23.6	12.9	11.6 <sup>f</sup>	474	60	(0.14, 0.22)	[62]

<sup>a</sup> Maximum EQE; <sup>b</sup> EQE at 1000 cd m<sup>-2</sup>; <sup>c</sup> Emission maximum; <sup>d</sup> LT<sub>50</sub> at 100 cd<sup>-2</sup>; <sup>e</sup> LT<sub>95</sub> at 1000 cd m<sup>-2</sup>; <sup>f</sup> LT<sub>90</sub> at 1000 cd m<sup>-2</sup>.

## References

- Tang, C.W.; Vanslyke, S.A. Organic electroluminescent diodes. *Appl. Phys. Lett.* **1987**, *51*, 913. [CrossRef]
- Friend, R.H.; Gymer, R.W.; Holmes, A.B.; Burroughes, J.H.; Marks, R.N.; Taliani, C.; Bradley, D.D.C.; Dos Santos, D.A.; Brédas, J.L.; Lögdlund, M.; et al. Electroluminescence in conjugated polymers. *Nature* **1999**, *397*, 121–128. [CrossRef]
- Park, I.S.; Komiyama, H.; Yasuda, T. Pyrimidine-based twisted donor–acceptor delayed fluorescence molecules: A new universal platform for highly efficient blue electroluminescence. *Chem. Sci.* **2016**, *8*, 953–960. [CrossRef]
- Lee, S.Y.; Adachi, C.; Yasuda, T. High-Efficiency Blue Organic Light-Emitting Diodes Based on Thermally Activated Delayed Fluorescence from Phenoxaphosphine and Phenoxathiin Derivatives. *Adv. Mater.* **2016**, *28*, 4626–4631. [CrossRef]
- Cha, J.-R.; Lee, C.W.; Lee, J.Y.; Gong, M.-S. Design of ortho-linkage carbazole-triazine structure for high-efficiency blue thermally activated delayed fluorescent emitters. *Dye. Pigment.* **2016**, *134*, 562–568. [CrossRef]

6. Sun, K.; Sun, Y.; Jiang, W.; Huang, S.; Tian, W.; Sun, Y. Highly efficient and color tunable thermally activated delayed fluorescent emitters and their applications for the solution-processed OLEDs. *Dye. Pigment.* **2017**, *139*, 326–333. [[CrossRef](#)]
7. Braveenth, R.; Chai, K.Y. Triazine-Acceptor-Based Green Thermally Activated Delayed Fluorescence Materials for Organic Light-Emitting Diodes. *Materials* **2019**, *12*, 2646. [[CrossRef](#)]
8. Chiu, T.-L.; Chuang, Y.-T. Spectral observations of hole injection with transition metal oxides for an efficient organic light-emitting diode. *J. Phys. D Appl. Phys.* **2015**, *48*, 075101. [[CrossRef](#)]
9. Bui, T.-T.; Goubard, F.; Ibrahim-Ouali, M.; Gigmès, D.; Dumur, F. Recent advances on organic blue thermally activated delayed fluorescence (TADF) emitters for organic light-emitting diodes (OLEDs). *Beilstein J. Org. Chem.* **2018**, *14*, 282–308. [[CrossRef](#)] [[PubMed](#)]
10. Reineke, S.; Thomschke, M.; Lüssem, B.; Leo, K. White organic light-emitting diodes: Status and perspective. *Rev. Mod. Phys.* **2013**, *85*, 1245–1293. [[CrossRef](#)]
11. Braveenth, R.; Bae, I.-J.; Wang, Y.; Kim, S.H.; Kim, M.; Chai, K.Y. Acridine-Triphenylamine Based Hole-Transporting and Hole-Injecting Material for Highly Efficient Phosphorescent-Based Organic Light Emitting Diodes. *Appl. Sci.* **2018**, *8*, 1168. [[CrossRef](#)]
12. Huh, D.H.; Kim, G.W.; Kulshreshtha, C.; Kwon, J.H. High hole mobility hole transport material for organic light-emitting devices. *Synth. Met.* **2013**, *180*, 79–84. [[CrossRef](#)]
13. Braveenth, R.; Bae, H.W.; Ko, I.J.; Qiong, W.; Nguyen, Q.P.B.; Jayashantha, P.G.S.; Kwon, J.H.; Chai, K.Y. Thermally stable efficient hole transporting materials based on carbazole and triphenylamine core for red phosphorescent OLEDs. *Org. Electron.* **2017**, *51*, 463–470. [[CrossRef](#)]
14. Zheng, Z.; Dong, Q.; Gou, L.; Su, J.-H.; Huang, J. Novel hole transport materials based on N,N'-disubstituted-dihydrophenazine derivatives for electroluminescent diodes. *J. Mater. Chem. C* **2014**, *2*, 9858–9865. [[CrossRef](#)]
15. Wei, Q.; Fei, N.; Islam, A.; Lei, T.; Hong, L.; Peng, R.; Fan, X.; Chen, L.; Gao, P.; Ge, Z. Small-Molecule Emitters with High Quantum Efficiency: Mechanisms, Structures, and Applications in OLED Devices. *Adv. Opt. Mater.* **2018**, *6*, 1800512. [[CrossRef](#)]
16. Baldo, M.A.; O'Brien, D.F.; Thompson, M.E.; Forrest, S.R. Excitonic singlet-triplet ratio in a semiconducting organic thin film. *Phys. Rev. B Condens. Matter Mater. Phys.* **1999**, *60*, 14422–14428. [[CrossRef](#)]
17. Forrest, S.; Bradley, D.; Thompson, M. Measuring the Efficiency of Organic Light-Emitting Devices. *Adv. Mater.* **2003**, *15*, 1043–1048. [[CrossRef](#)]
18. Reineke, S.; Lindner, F.; Schwartz, G.; Seidler, N.; Walzer, K.; Lüssem, B.; Leo, K. White organic light-emitting diodes with fluorescent tube efficiency. *Nature* **2009**, *459*, 234–238. [[CrossRef](#)] [[PubMed](#)]
19. Baldo, M.A.; O'Brien, D.F.; You, Y.; Shoustikov, A.; Sibley, S.; Thompson, M.E.; Forrest, S.R. Highly efficient phosphorescent emission from organic electroluminescent devices. *Nature* **1998**, *395*, 151–154. [[CrossRef](#)]
20. Baldo, M.A.; Adachi, C.; Forrest, S.R. Transient analysis of organic electrophosphorescence. II. Transient analysis of triplet-triplet annihilation. *Phys. Rev. B* **2000**, *62*, 10967. [[CrossRef](#)]
21. Ganzorig, C.; Fujihira, M. A possible mechanism for enhanced electrofluorescence emission through triplet-triplet annihilation in organic electroluminescent devices. *Appl. Phys. Lett.* **2002**, *81*, 3137–3139. [[CrossRef](#)]
22. Leitl, M.J.; Zink, D.M.; Schinabeck, A.; Baumann, T.; Volz, D.; Yersin, H. Copper(I) Complexes for Thermally Activated Delayed Fluorescence: From Photophysical to Device Properties. *Top. Curr. Chem.* **2016**, *374*, 25. [[CrossRef](#)] [[PubMed](#)]
23. Uoyama, H.; Goushi, K.; Shizu, K.; Nomura, H.; Adachi, C. Highly efficient organic light-emitting diodes from delayed fluorescence. *Nature* **2012**, *492*, 234–238. [[CrossRef](#)]
24. Liu, Y.; Li, C.; Ren, Z.; Yan, S.; Bryce, M.R. All-organic thermally activated delayed fluorescence materials for organic light-emitting diodes. *Nat. Rev. Mater.* **2018**, *3*, 18020. [[CrossRef](#)]
25. Lin, C.-C.; Huang, M.-J.; Chiu, M.-J.; Huang, M.-P.; Chang, C.-C.; Liao, C.-Y.; Chiang, K.-M.; Shiau, Y.-J.; Chou, T.-Y.; Chu, L.-K.; et al. Molecular Design of Highly Efficient Thermally Activated Delayed Fluorescence Hosts for Blue Phosphorescent and Fluorescent Organic Light-Emitting Diodes. *Chem. Mater.* **2017**, *29*, 1527–1537. [[CrossRef](#)]
26. Huang, T.; Jiang, W.; Duan, L. Recent progress in solution processable TADF materials for organic light-emitting diodes. *J. Mater. Chem. C* **2018**, *6*, 5577–5596. [[CrossRef](#)]
27. Komatsu, R.; Sasabe, H.; Nakao, K.; Hayasaka, Y.; Ohsawa, T.; Kido, J. Unlocking the Potential of Pyrimidine Conjugate Emitters to Realize High-Performance Organic Light-Emitting Devices. *Adv. Opt. Mater.* **2017**, *5*, 1600675. [[CrossRef](#)]
28. Liang, X.; Tu, Z.; Zheng, Y. Thermally Activated Delayed Fluorescence Materials: Towards Realization of High Efficiency through Strategic Small Molecular Design. *Chem. Eur. J.* **2019**, *25*, 5623–5642. [[CrossRef](#)]
29. Kitamoto, Y.; Namikawa, T.; Suzuki, T.; Miyata, Y.; Kita, H.; Sato, T.; Oi, S. Design and synthesis of efficient blue thermally activated delayed fluorescence molecules bearing triarylborane and 10,10-dimethyl-5,10-dihydrophenazasiline moieties. *Tetrahedron Lett.* **2016**, *57*, 4914–4917. [[CrossRef](#)]
30. Cai, X.; Su, S.-J. Marching Toward Highly Efficient, Pure-Blue, and Stable Thermally Activated Delayed Fluorescent Organic Light-Emitting Diodes. *Adv. Funct. Mater.* **2018**, *28*, 1802558. [[CrossRef](#)]
31. Hatakeyama, T.; Shiren, K.; Nakajima, K.; Nomura, S.; Nakatsuka, S.; Kinoshita, K.; Ni, J.; Ono, Y.; Ikuta, T. Ultrapure Blue Thermally Activated Delayed Fluorescence Molecules: Efficient HOMO-LUMO Separation by the Multiple Resonance Effect. *Adv. Mater.* **2016**, *28*, 2777–2781. [[CrossRef](#)]

32. Matsui, K.; Oda, S.; Yoshiura, K.; Nakajima, K.; Yasuda, N.; Hatakeyama, T. One-Shot Multiple Borylation toward BN-Doped Nanographenes. *J. Am. Chem. Soc.* **2018**, *140*, 1195–1198. [[CrossRef](#)]
33. Oda, S.; Sugitani, T.; Tanaka, H.; Tabata, K.; Kawasumi, R.; Hatakeyama, T. Development of Pure Green Thermally Activated Delayed Fluorescence Material by Cyano Substitution. *Adv. Mater.* **2022**, *34*, 2201778. [[CrossRef](#)]
34. Lee, H.; Karthik, D.; Lampande, R.; Ryu, J.H.; Kwon, J.H. Recent Advancement in Boron-Based Efficient and Pure Blue Thermally Activated Delayed Fluorescence Materials for Organic Light-Emitting Diodes. *Front. Chem.* **2020**, *8*, 373. [[CrossRef](#)]
35. Kondo, Y.; Yoshiura, K.; Kitera, S.; Nishi, H.; Oda, S.; Gotoh, H.; Sasada, Y.; Yanai, M.; Hatakeyama, T. Narrowband deep-blue organic light-emitting diode featuring an organoboron-based emitter. *Nat. Photonics* **2019**, *13*, 678–682. [[CrossRef](#)]
36. Chan, C.-Y.; Tanaka, M.; Lee, Y.-T.; Wong, Y.-W.; Nakanotani, H.; Hatakeyama, T.; Adachi, C. Stable pure-blue hyperfluorescence organic light-emitting diodes with high-efficiency and narrow emission. *Nat. Photonics* **2021**, *15*, 203–207. [[CrossRef](#)]
37. Jeon, S.O.; Lee, K.H.; Kim, J.S.; Ihn, S.-G.; Chung, Y.S.; Kim, J.W.; Lee, H.; Kim, S.; Choi, H.; Lee, J.Y. High-efficiency, long-lifetime deep-blue organic light-emitting diodes. *Nat. Photonics* **2021**, *15*, 208–215. [[CrossRef](#)]
38. Lo, K.; Tong, G.S.M.; Cheng, G.; Low, K.; Che, C. Dinuclear Pt II Complexes with Strong Blue Phosphorescence for Operationally Stable Organic Light-Emitting Diodes with EQE up to 23% at 1000 cd m<sup>-2</sup>. *Angew. Chem. Int. Ed.* **2022**, *61*, e202115515. [[CrossRef](#)]
39. Huang, T.; Wang, Q.; Meng, G.; Duan, L.; Zhang, D. Accelerating Radiative Decay in Blue Through-Space Charge Transfer Emitters by Minimizing the Face-to-Face Donor-Acceptor Distances. *Angew. Chem. Int. Ed.* **2022**, *61*, e202200059. [[CrossRef](#)]
40. Zhou, D.; Wu, S.; Cheng, G.; Che, C.-M. A gold(III)-TADF emitter as a sensitizer for high-color-purity and efficient deep-blue solution-processed OLEDs. *J. Mater. Chem. C* **2022**, *10*, 4590–4596. [[CrossRef](#)]
41. Zhang, Y.; Zhang, D.; Wei, J.; Hong, X.; Lu, Y.; Hu, D.; Li, G.; Liu, Z.; Chen, Y.; Duan, L. Achieving Pure Green Electroluminescence with CIEy of 0.69 and EQE of 28.2% from an Aza-Fused Multi-Resonance Emitter. *Angew. Chem. Int. Ed.* **2020**, *59*, 17499–17503. [[CrossRef](#)]
42. Yang, M.; Shikita, S.; Min, H.; Park, I.S.; Shibata, H.; Amanokura, N.; Yasuda, T. Wide-Range Color Tuning of Narrowband Emission in Multi-resonance Organoboron Delayed Fluorescence Materials through Rational Imine/Amine Functionalization. *Angew. Chem. Int. Ed.* **2021**, *60*, 23142–23147. [[CrossRef](#)]
43. Jiang, P.; Miao, J.; Cao, X.; Xia, H.; Pan, K.; Hua, T.; Lv, X.; Huang, Z.; Zou, Y.; Yang, C. Quenching-Resistant Multiresonance TADF Emitter Realizes 40% External Quantum Efficiency in Narrowband Electroluminescence at High Doping Level. *Adv. Mater.* **2022**, *34*, 2106954. [[CrossRef](#)]
44. Bian, J.; Chen, S.; Qiu, L.; Tian, R.; Man, Y.; Wang, Y.; Chen, S.; Zhang, J.; Duan, C.; Han, C.; et al. Ambipolar Self-Host Functionalization Accelerates Blue Multi-Resonance Thermally Activated Delayed Fluorescence with Internal Quantum Efficiency of 100%. *Adv. Mater.* **2022**, *34*, 2110547. [[CrossRef](#)]
45. Lv, X.; Miao, J.; Liu, M.; Peng, Q.; Zhong, C.; Hu, Y.; Cao, X.; Wu, H.; Yang, Y.; Zhou, C.; et al. Extending the  $\pi$ -Skeleton of Multi-Resonance TADF Materials towards High-Efficiency Narrowband Deep-Blue Emission. *Angew. Chem. Int. Ed.* **2022**, *61*, e202201588. [[CrossRef](#)]
46. Pershin, A.; Hall, D.; Lemaire, V.; Sancho-Garcia, J.-C.; Muccioli, L.; Zysman-Colman, E.; Beljonne, D.; Olivier, Y. Highly emissive excitons with reduced exchange energy in thermally activated delayed fluorescent molecules. *Nat. Commun.* **2019**, *10*, 597. [[CrossRef](#)]
47. Xia, D.; Wang, B.; Chen, B.; Wang, S.; Zhang, B.; Ding, J.; Wang, L.; Jing, X.; Wang, F. Self-Host Blue-Emitting Iridium Dendrimer with Carbazole Dendrons: Nondoped Phosphorescent Organic Light-Emitting Diodes. *Angew. Chem. Int. Ed.* **2014**, *53*, 1048–1052. [[CrossRef](#)]
48. Xu, Y.; Cheng, Z.; Li, Z.; Liang, B.; Wang, J.; Wei, J.; Zhang, Z.; Wang, Y. Molecular-Structure and Device-Configuration Optimizations toward Highly Efficient Green Electroluminescence with Narrowband Emission and High Color Purity. *Adv. Opt. Mater.* **2020**, *8*, 1902142. [[CrossRef](#)]
49. Park, J.; Kim, K.J.; Lim, J.; Kim, T.; Lee, J.Y. High Efficiency of over 25% and Long Device Lifetime of over 500 h at 1000 nit in Blue Fluorescent Organic Light-Emitting Diodes. *Adv. Mater.* **2022**, *34*, 2108581. [[CrossRef](#)]
50. Han, S.H.; Jeong, J.H.; Yoo, J.W.; Lee, J.Y. Ideal blue thermally activated delayed fluorescence emission assisted by a thermally activated delayed fluorescence assistant dopant through a fast reverse intersystem crossing mediated cascade energy transfer process. *J. Mater. Chem. C* **2019**, *7*, 3082–3089. [[CrossRef](#)]
51. Xue, Q.; Xie, G. Thermally Activated Delayed Fluorescence beyond Through-Bond Charge Transfer for High-Performance OLEDs. *Adv. Opt. Mater.* **2021**, *9*, 2002204. [[CrossRef](#)]
52. Chen, X.-K.; Bakr, B.W.; Auffray, M.; Tsuchiya, Y.; Sherrill, C.D.; Adachi, C.; Bredas, J.-L. Intramolecular Noncovalent Interactions Facilitate Thermally Activated Delayed Fluorescence (TADF). *J. Phys. Chem. Lett.* **2019**, *10*, 3260–3268. [[CrossRef](#)]
53. Wu, C.; Liu, W.; Li, K.; Cheng, G.; Xiong, J.; Teng, T.; Che, C.; Yang, C. Face-to-Face Orientation of Quasiplanar Donor and Acceptor Enables Highly Efficient Intramolecular Exciplex Fluorescence. *Angew. Chem. Int. Ed.* **2021**, *60*, 3994–3998. [[CrossRef](#)]
54. Tsujimoto, H.; Ha, D.-G.; Markopoulos, G.; Chae, H.S.; Baldo, M.A.; Swager, T.M. Thermally Activated Delayed Fluorescence and Aggregation Induced Emission with Through-Space Charge Transfer. *J. Am. Chem. Soc.* **2017**, *139*, 4894–4900. [[CrossRef](#)]
55. Wada, Y.; Nakagawa, H.; Matsumoto, S.; Wakisaka, Y.; Kaji, H. Organic light emitters exhibiting very fast reverse intersystem crossing. *Nat. Photonics* **2020**, *14*, 643–649. [[CrossRef](#)]
56. Peng, C.; Yang, S.; Li, H.; Xie, G.; Cui, L.; Zou, S.; Poriel, C.; Jiang, Z.; Liao, L. Highly Efficient Thermally Activated Delayed Fluorescence via an Unconjugated Donor-Acceptor System Realizing EQE of Over 30%. *Adv. Mater.* **2020**, *32*, e2003885. [[CrossRef](#)]

57. Tang, X.; Cui, L.-S.; Li, H.-C.; Gillett, A.J.; Auras, F.; Qu, Y.-K.; Zhong, C.; Jones, S.T.E.; Jiang, Z.-Q.; Friend, R.H.; et al. Highly efficient luminescence from space-confined charge-transfer emitters. *Nat. Mater.* **2020**, *19*, 1332–1338. [[CrossRef](#)]
58. Wang, X.; Yang, S.; Tian, Q.; Zhong, C.; Qu, Y.; Yu, Y.; Jiang, Z.; Liao, L. Multi-Layer  $\pi$ -Stacked Molecules as Efficient Thermally Activated Delayed Fluorescence Emitters. *Angew. Chem. Int. Ed.* **2020**, *60*, 5213–5219. [[CrossRef](#)]
59. Shao, S.; Hu, J.; Wang, X.; Wang, L.; Jing, X.; Wang, F. Blue Thermally Activated Delayed Fluorescence Polymers with Nonconjugated Backbone and Through-Space Charge Transfer Effect. *J. Am. Chem. Soc.* **2017**, *139*, 17739–17742. [[CrossRef](#)]
60. Zhao, Z.; Zeng, C.; Peng, X.; Liu, Y.; Zhao, H.; Hua, L.; Su, S.-J.; Yan, S.; Ren, Z. Tuning Intramolecular Stacking of Rigid Heteroaromatic Compounds for High-Efficiency Deep-blue Through-Space Charge-Transfer Emission. *Angew. Chem. Int. Ed.* **2022**, *61*, e202210864. [[CrossRef](#)]
61. Yang, Z.; Mao, Z.; Xie, Z.; Zhang, Y.; Liu, S.; Zhao, J.; Xu, J.; Chi, Z.; Aldred, M.P. Recent advances in organic thermally activated delayed fluorescence materials. *Chem. Soc. Rev.* **2017**, *46*, 915–1016. [[CrossRef](#)] [[PubMed](#)]
62. Tang, R.; Xu, S.; Lam, T.; Cheng, G.; Du, L.; Wan, Q.; Yang, J.; Hung, F.; Low, K.; Phillips, D.L.; et al. Highly Robust Cu I-TADF Emitters for Vacuum-Deposited OLEDs with Luminance up to 222 200  $\text{cd m}^{-2}$  and Device Lifetimes ( $\text{LT}_{90}$ ) up to 1300 h at an Initial Luminance of 1000  $\text{cd m}^{-2}$ . *Angew. Chem. Int. Ed.* **2022**, *61*, e202203982. [[CrossRef](#)]
63. Czerwieńiec, R.; Yu, J.; Yersin, H. Blue-Light Emission of Cu(I) Complexes and Singlet Harvesting. *Inorg. Chem.* **2011**, *50*, 8293–8301. [[CrossRef](#)] [[PubMed](#)]
64. Czerwieńiec, R.; Leitl, M.J.; Homeier, H.H.; Yersin, H. Cu(I) complexes—Thermally activated delayed fluorescence. Photophysical approach and material design. *Coord. Chem. Rev.* **2016**, *325*, 2–28. [[CrossRef](#)]
65. Yersin, H.; Czerwieńiec, R.; Shafikov, M.Z.; Suleymanova, A.F. TADF Material Design: Photophysical Background and Case Studies Focusing on  $\text{Cu}^{\text{I}}$  and  $\text{Ag}^{\text{I}}$  Complexes. *ChemPhysChem* **2017**, *18*, 3508–3535. [[CrossRef](#)]
66. To, W.-P.; Cheng, G.; Tong, G.S.M.; Zhou, D.; Che, C.-M. Recent Advances in Metal-TADF Emitters and Their Application in Organic Light-Emitting Diodes. *Front. Chem.* **2020**, *8*, 653. [[CrossRef](#)]
67. Di, D.; Romanov, A.S.; Yang, L.; Richter, J.M.; Rivett, J.P.H.; Jones, S.; Thomas, T.H.; Jalebi, M.A.; Friend, R.H.; Linnolahti, M.; et al. High-performance light-emitting diodes based on carbene-metal-amides. *Science* **2017**, *356*, 159–163. [[CrossRef](#)]
68. Zhou, D.; To, W.; Tong, G.S.M.; Cheng, G.; Du, L.; Phillips, D.L.; Che, C. Tetradentate Gold(III) Complexes as Thermally Activated Delayed Fluorescence (TADF) Emitters: Microwave-Assisted Synthesis and High-Performance OLEDs with Long Operational Lifetime. *Angew. Chem. Int. Ed.* **2020**, *59*, 6375–6382. [[CrossRef](#)]
69. Malmberg, R.; Venkatesan, K. Recent Advances in the Development of Blue and Deep-Blue Emitting Gold(I) and Gold(III) Molecular Systems. *Eur. J. Inorg. Chem.* **2021**, *2021*, 4890–4902. [[CrossRef](#)]
70. Shi, S.; Jung, M.C.; Coburn, C.; Tadde, A.; Sylvinson, M.R.D.; Djurovich, P.I.; Forrest, S.R.; Thompson, M.E. Highly Efficient Photo- and Electroluminescence from Two-Coordinate Cu(I) Complexes Featuring Nonconventional N-Heterocyclic Carbenes. *J. Am. Chem. Soc.* **2019**, *141*, 3576–3588. [[CrossRef](#)]
71. Conaghan, P.J.; Matthews, C.S.B.; Chotard, F.; Jones, S.T.E.; Greenham, N.C.; Bochmann, M.; Credgington, D.; Romanov, A.S. Highly efficient blue organic light-emitting diodes based on carbene-metal-amides. *Nat. Commun.* **2020**, *11*, 1758. [[CrossRef](#)] [[PubMed](#)]
72. Zhou, D.; Cheng, G.; Tong, G.S.M.; Che, C. High Efficiency Sky-Blue Gold(III)-TADF Emitters. *Chem. Eur. J.* **2020**, *26*, 15718–15726. [[CrossRef](#)]
73. To, W.-P.; Zhou, D.; Tong, G.S.M.; Cheng, G.; Yang, C.; Che, C.-M. Highly Luminescent Pincer Gold(III) Aryl Emitters: Thermally Activated Delayed Fluorescence and Solution-Processed OLEDs. *Angew. Chem. Int. Ed.* **2017**, *56*, 14036–14041. [[CrossRef](#)] [[PubMed](#)]
74. Ying, A.; Huang, Y.-H.; Lu, C.-H.; Chen, Z.; Lee, W.-K.; Zeng, X.; Chen, T.; Cao, X.; Wu, C.-C.; Gong, S.; et al. High-Efficiency Red Electroluminescence Based on a Carbene-Cu(I)-Acridine Complex. *ACS Appl. Mater. Interfaces* **2021**, *13*, 13478–13486. [[CrossRef](#)]
75. Liu, Z.; Qiu, J.; Wei, F.; Wang, J.; Liu, X.; Helander, M.G.; Rodney, S.; Wang, Z.; Bian, Z.; Lu, Z.; et al. Simple and High Efficiency Phosphorescence Organic Light-Emitting Diodes with Codeposited Copper(I) Emitter. *Chem. Mater.* **2014**, *26*, 2368–2373. [[CrossRef](#)]
76. Hamze, R.; Peltier, J.L.; Sylvinson, D.; Jung, M.; Cardenas, J.; Haiges, R.; Soleilhavoup, M.; Jazsar, R.; Djurovich, P.I.; Bertrand, G.; et al. Eliminating nonradiative decay in Cu(I) emitters: >99% quantum efficiency and microsecond lifetime. *Science* **2019**, *363*, 601–606. [[CrossRef](#)]
77. Xie, M.; Han, C.; Liang, Q.; Zhang, J.; Xie, G.; Xu, H. Highly efficient sky blue electroluminescence from ligand-activated copper iodide clusters: Overcoming the limitations of cluster light-emitting diodes. *Sci. Adv.* **2019**, *5*, eaav9857. [[CrossRef](#)]
78. Murawski, C.; Leo, K.; Gather, M.C. Efficiency Roll-Off in Organic Light-Emitting Diodes. *Adv. Mater.* **2013**, *25*, 6801–6827. [[CrossRef](#)]
79. Schmidbauer, S.; Hohenleutner, A.; König, B. Chemical Degradation in Organic Light-Emitting Devices: Mechanisms and Implications for the Design of New Materials. *Adv. Mater.* **2013**, *25*, 2114–2129. [[CrossRef](#)]
80. Yersin, H.; Mataranga-Popa, L.; Czerwieńiec, R.; Dovbii, Y. Design of a New Mechanism beyond Thermally Activated Delayed Fluorescence toward Fourth Generation Organic Light Emitting Diodes. *Chem. Mater.* **2019**, *31*, 6110–6116. [[CrossRef](#)]
81. Yersin, H.; Czerwieńiec, R.; Mataranga-Popa, L.; Mewes, J.; Cheng, G.; Che, C.; Saigo, M.; Kimura, S.; Miyata, K.; Onda, K. Eliminating the Reverse ISC Bottleneck of TADF Through Excited State Engineering and Environment-Tuning toward State

- Resonance Leading to Mono-Exponential Sub- $\mu$ s Decay. High OLED External Quantum Efficiency Confirms Efficient Exciton Harvesting. *Adv. Funct. Mater.* **2022**, *32*, 2201772. [[CrossRef](#)]
82. Aizawa, N.; Pu, Y.-J.; Harabuchi, Y.; Nihonyanagi, A.; Ibuka, R.; Inuzuka, H.; Dhara, B.; Koyama, Y.; Nakayama, K.-I.; Maeda, S.; et al. Delayed fluorescence from inverted singlet and triplet excited states. *Nature* **2022**, *609*, 502–506. [[CrossRef](#)]
83. Audebert, P.; Kroke, E.; Posern, C.; Lee, S.-H. State of the Art in the Preparation and Properties of Molecular Monomeric *s*-Heptazines: Syntheses, Characteristics, and Functional Applications. *Chem. Rev.* **2021**, *121*, 2515–2544. [[CrossRef](#)] [[PubMed](#)]
84. de Silva, P. Inverted Singlet-Triplet Gaps and Their Relevance to Thermally Activated Delayed Fluorescence. *J. Phys. Chem. Lett.* **2019**, *10*, 5674–5679. [[CrossRef](#)] [[PubMed](#)]
85. Sanz-Rodrigo, J.; Ricci, G.; Olivier, Y.; Sancho-García, J.C. Negative Singlet-Triplet Excitation Energy Gap in Triangle-Shaped Molecular Emitters for Efficient Triplet Harvesting. *J. Phys. Chem. A* **2021**, *125*, 513–522. [[CrossRef](#)] [[PubMed](#)]
86. Pollice, R.; Friederich, P.; Lavigne, C.; Gomes, G.D.P.; Aspuru-Guzik, A. Organic molecules with inverted gaps between first excited singlet and triplet states and appreciable fluorescence rates. *Matter* **2021**, *4*, 1654–1682. [[CrossRef](#)]